Available online at www.sciencedirect.com
ScienceDirect
Journal of Hydrodynamics
2009,21(3):394-400
DOI: 10.1016/S1001-6058(08)60162-6
www.sciencedirect.com/science/journal/10016058

THE INFLUENCE OF DIFFERENT DESIGN PARAMETERS AND WORKING CONDITIONS ON CHARACTERISTICS OF HEAT METERS*

LIU Yong-hui, DU Guang-sheng , LIU Zheng-gang, WANG You-yuan
School of Energy and Power Engineering, Shandong University, Jinan 250061 China,
E-mail: liu@mail.sdu.edu.cn

(Received June 15, 2008, Revised August 10, 2008)

Abstract: In this article, the UDF technology in Fluent software is used to simulate three-dimensional flow fields and to obtain various flow parameters. The standard $k-\varepsilon$ model and the RNG $k-\varepsilon$ model are both used to calculate the inner flow field of the basal meter, and a comparison of the calculated results between two models shows that RNG $k-\varepsilon$ model is more effective for calculations of the inner flow of rotary wing mechanism. The influence of tip clearance on the characteristics of the basal meter is studied. The influence of the bottom ribs on the heat meter is evaluated by the numerical simulation method. This article also simulates the flow of disturbance located at the inlet of the basal meter, and shows that a swirl located at the front of the basal meter can affect the stability of the heat meter.

Key words: two-channel, heat meter, numerical simulation, tip clearance

1. Introduction

The heat meter is finding wide applications with the reform of the charge method in the winter heating system and various heat meters are being produced. Compared with the foreign made products, the technology and the measurement accuracy of the homemade heat meters are not adequate[1-4].

At present, the impeller mechanism has been much studied. In Refs.[5-7], the $k-\varepsilon$ model is used to simulate Francis turbine, vortex pump and cyclone separators. It is shown that the $k-\varepsilon$ model is effective for calculations of the inner flow of the impeller mechanism. The working of a heat meter is very much related with the impeller mechanism. In Refs.[8,9], the standard $k-\varepsilon$ model is used to study the influence of the number of vanes, temperature, the adjusting ribbed plate and inlet straight pipe on characteristics of single-channel heat meters, in the Refs.[10-12], the standard $k-\varepsilon$ model is used to calculate the rotational speed of impeller, pressure loss and the influence of deflector. These numerical simulations suffer from some drawbacks: (1) with the use of the standard $k-\varepsilon$ model, the relative error between calculation and experiment is large (7.8% in Ref.[11]), (2) the rotational speed of impeller is obtained by iterative calculations, involving a long calculation period, (3) some parameters including tip clearance, bottom ribs and inlet swirls are not included in the simulations.

This article will deal with these problems. First, a new method to calculate the rotational speed of impeller is developed by using the User Define Function (UDF for short) technology, to obtain the speed directly. Second, the standard $k-\varepsilon$ model and the RNG $k-\varepsilon$ model are both used to make calculations for the heat meter and the selection of models are determined by comparing the calculation results with the experimental results. Finally, the influences of tip clearance, bottom ribs and the inlet swirl on characteristics of the heat meters are analyzed.

* **Biography:** LIU Yong-hui (1981-), Male, Ph. D. Candidate

2. Physical model

The physical model is a two-channel rotary wing heat meter. The nominal diameter is 0.02 m, the standard rated flow is 2.5 m^3/h and the medium is water. Because water temperature hardly influences the measurement accuracy of the heat meter [8], its influence is ignored here and the normal temperature is adopted.

The parts of the basal meter are shown in Fig.1, including base frame, chamber, impeller and upper cover.

Fig.1 Parts of basal meter

The model of the basal meter is built by Pro/E software, as shown in Fig.2. In order to ensure the stability of inner flow, the inlet straight tube of the model is four times as long as the pipe diameter and the outlet straight tube is seven times as long[9].

Fig.2 Physical model

3. Mathematical model

In this article, the standard $k-\varepsilon$ model and the RNG $k-\varepsilon$ model are both used in the calculation, and the selection of a better model is determined by comparing two calculation results with the experimental results.

3.1 *Basic control equation*[13,14]

Continuity equation:

$$\frac{\partial \rho}{\partial t}+\frac{\rho \partial(u_i)}{\partial x_i}=0 \tag{1}$$

Momentum equation:

$$\frac{\partial(\rho u_i)}{\partial t}+\frac{\partial(\rho \overline{u}_i \overline{u}_j)}{\partial x_j}=-\frac{\partial \overline{p}}{\partial x_i}+\frac{\partial}{\partial x_j}\bullet$$

$$\left(\mu\frac{\partial \overline{u}_i}{\partial x_j}-\rho\overline{u_i' u_j'}\right) \tag{2}$$

Viscosity coefficient of turbulence:

$$\mu_t=\frac{\rho C_\mu k^2}{\varepsilon} \tag{3}$$

where ρ is the density of water, $\overline{u}$ is the velocity of flow, the symbol "—" above variables means averaging over time, P is pressure, μ is the viscosity coefficient.

3.2 *The standard* $k-\varepsilon$ *model*[13-16]

k equation:

$$\frac{\partial(\rho k)}{\partial t}+\frac{\partial(\rho k u_i)}{\partial x_i}=\frac{\partial}{\partial x_j}\left[\left(\mu+\frac{\mu_t}{\sigma_k}\right)\frac{\partial k}{\partial x_j}\right]+$$

$$G_k+G_b-\rho\varepsilon-Y_M+S \tag{4}$$

ε equation:

$$\frac{\partial(\rho \varepsilon)}{\partial t}+\frac{\partial}{\partial x_i}(\rho \varepsilon u_i)=\frac{\partial}{\partial x_j}\left[\left(\mu+\frac{\mu_t}{\sigma_\varepsilon}\right)\frac{\partial \varepsilon}{\partial x_j}\right]+$$

$$C_{1\varepsilon}\frac{\varepsilon}{k}(G_k+C_{3\varepsilon}G_b)-C_{2\varepsilon}\rho\frac{\varepsilon^2}{k}+S_\varepsilon \tag{5}$$

where G_k is the turbulent kinetic energy produced by the gradient of the average velocity, G_b is the turbulence kinetic energy produced by the flotage, Y_M expresses the panting action caused by the diffusivity of the compressible turbulent flow, $C_{1\varepsilon}$, $C_{2\varepsilon}$ and $C_{3\varepsilon}$ are constant coefficients, σ_K and σ_ε are the turbulent Prandtl numbers related with k and ε coefficients, S_K and S_ε are user-defined source terms.

The turbulent kinetic energy G_b and related coefficients $C_{3\varepsilon}$ produced by the flotage are considered for compressible flows. When the fluid is

incompressible and the user-defined source terms are not considered, G_b, Y_M, S_K and S_ε are equal to zero. The values of constant coefficients $C_{1\varepsilon}, C_{2\varepsilon}, C_\mu$ and σ_K, σ_ε are: $C_{1\varepsilon}=1.44$, $C_{2\varepsilon}=1.92$, $C_\mu=0.09$, $\sigma_k=1.0$, $\sigma_\varepsilon=1.3$.

3.3 *The RNG $k-\varepsilon$ model [13,15-17]*

Compared to the standard $k-\varepsilon$ model, the major changes made in the RNG $k-\varepsilon$ model are: (1) the rotational flow is considered by correcting the turbulence viscosity, (2) in ε equation, one item is added to express the strain ratio in average time, E_{ij}. The RNG $k-\varepsilon$ model is not only related to the flow, but also to the deformation in space. So the RNG $k-\varepsilon$ model is more effective for problems with high strain ratio flow and high degrees of curvature of streamline. The inner structure of the basal meter is complex, and swirls of different dimensions are easy to form, so the RNG $k-\varepsilon$ model should be more effective for the heat meter calculation, theoretically speaking.

k equation:

$$\frac{\partial(\rho k)}{\partial t}+\frac{\partial}{\partial x_i}\left(\rho k u_i\right)=\frac{\partial}{\partial x_j}\left[\alpha_k \mu_{eff}\frac{\partial k}{\partial x_j}\right]+ G_k+G_b-\rho\varepsilon-Y_M+S_k \tag{6}$$

ε equation:

$$\frac{\partial(\rho \varepsilon)}{\partial t}+\frac{\partial}{\partial x_i}\left(\rho \varepsilon u_i\right)=\frac{\partial}{\partial x_j}\left[\alpha_k \mu_{eff}\frac{\partial \varepsilon}{\partial x_j}\right]+ \frac{C_{1\varepsilon}^*}{k}G_k-\mathrm{C}_{2\varepsilon}\rho\frac{\varepsilon^2}{k}+S_\varepsilon \tag{7}$$

where

$$\mu_{eff}=\mu+\mu_t,\quad \mu_t=\frac{\rho C_\mu k^2}{\varepsilon},$$

$$C_\mu=0.0845,\ \alpha_k=1.39,\ C_{1\varepsilon}=1.42,$$

$$C_{2\varepsilon}=1.68,\ C_{1\varepsilon}^*=C_{1\varepsilon}-\frac{\eta\left(1-\eta/\eta_0\right)}{1+\beta\eta^3},$$

$$\eta=(2E_{ij}E_{ij})^{1/2}\frac{k}{\varepsilon},\quad E_{ij}=\frac{1}{2}\left(\frac{\partial u_i}{\partial x_i}+\frac{\partial u_j}{\partial x_i}\right),$$

$$\eta_0=4.377,\ \beta=0.012$$

4. Numerical Simulation

4.1 *Calculation mesh*

Sliding mesh is used to deal with the rotation of impeller. Stator and rotor meshes are generated, respectively, by Gambit software, combined with Fluent software. The models of rotor and stator are shown in Fig.3 and Fig.4.

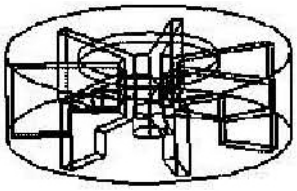

Fig.3 Rotor model

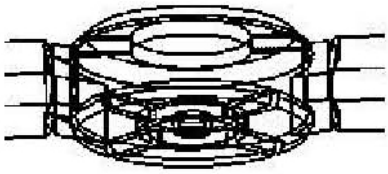

Fig.4 Stator model

4.2 *Boundary conditions and near-wall treatments*

A mass-flow-inlet condition is adopted at the inlet of the calculation domain. Because of incompressibility of water, the mass-flow-inlet condition is the same as the velocity inlet condition. The pressure-outlet condition is adopted at the outlet.

The standard wall function is adopted to deal with the near-wall region[15].

4.3 *Turbulent parameters*

In this article, intensity and hydraulic diameter are used to describe turbulence, and the calculation formula[15] is:

$$I=\frac{\overline{u'^2}}{u_{avg}}\cong 0.16\left(Re_{D_H}\right)^{-1/8} \tag{8}$$

where $\overline{u'^2}$ is the root-mean-square of velocity fluctuation, u_{avg} is the average velocity.

In this calculation, flux $Q=2.5\mathrm{m}^3/\mathrm{h}$, pipe diameter $D=0.02\mathrm{m}$. For the pipe, $D_H=D$.

$$Re_{D_H} = \frac{vl}{\nu} = \frac{QD}{3600 \times A\nu} = 4.2 \times 10^4,$$

$$I = \frac{\overline{u'^2}}{u_{avg}} \cong 0.16\left(Re_{D_H}\right)^{-1/8} = 4.2\%$$

4.4 *Calculation of the impeller speed*

In this article, UDF technology is used to calculate the impeller speed. UDF is a method with a user defined function, programmed in C language.

The calculation of the impeller speed is based upon the equation of moment balance $J\alpha = M$. First, a start speed ω_0 is given at the beginning of calculation, and $\omega = \omega_0$. Second, the impeller moment M is calculated through numerical calculations when the impeller rotates one time step, t. Third, the angular acceleration α is obtained through the moment balance equation $J\alpha = M$, where J is the moment of inertia. Then, the next step speed ω_1 is obtained from the acceleration equation $\omega_{n+1} = \omega_n + \alpha t$. Repeat the above process till the speed is steady or varying periodically. This speed is taken as the impeller rotational speed.

5. Experiments

5.1 *Objectives of experiments*

The meter coefficient, K, is a basic parameter of the heat meter. Theoretically, it is a constant, defined as[10]:

$$K = \frac{f}{Q_v} \tag{9}$$

where K is meter coefficient (pulse/liter), f is the number of pulse signals in one unit of time, Q_v is flux. The rotational speed of the impeller, *n*, is directly proportional to K:

$$n = \frac{K}{240} Q \tag{10}$$

where n is the rotational speed of the impeller, Q is the flux flowing through the basal meter.

Another basic parameter of the heat meter is the pressure loss between inlet and outlet. According to the regulation of CJ128-2007, the pressure loss should be less than 25 KPa.

In this article the rotational speed of the impeller and the pressure loss with different design parameters are determined by experiments. Design parameters include tip clearance and bottom ribs.

5.2 *Experimental equipment*

The details of experimental equipment and experimental method are described in Refs.[8-12].

6. Analysis of experimental and numerical simulation results

6.1 *Comparison of different models*

At the flux of 2.5 m^3/h, the standard $k-\varepsilon$ model and the RNG $k-\varepsilon$ model are separately used in calculation and the results are compared with experimental results, as shown in Table 1:

Table 1 Comparison of different models

Model	Pressure loss (KPa)	Rotational speed (rpm)
RNG $k-\varepsilon$	19.4	600
Standard $k-\varepsilon$	18	567
Experiment	19.6	623

In this article, the impeller rotational speed is 567 rpm obtained with the standard $k-\varepsilon$ model by the method of UDF technology, and the speed is 562.7 rpm in Ref.[11] obtained by the method of iterative calculation. The results of two methods are consistent, which validates the method of UDF technology.

The calculation errors of pressure loss and rotational speed obtained with different models as compared with experiments are as follows: with the RNG $k-\varepsilon$ model, errors are 1.0% and 3.7%, and with the standard $k-\varepsilon$ model, errors are 8.1% and 8.9%. It is obvious that the results calculated with the RNG $k-\varepsilon$ model are closer to the experimental values. From the analysis of Section 3.3, and this comparison, it can be concluded that the RNG $k-\varepsilon$ model is more effective to solve problems with high strain ratio flow and high degree of curvature of streamline. So, in this article, the RNG $k-\varepsilon$ model will be used in all calculations.

6.2 *Influence of tip clearance*

Tip clearance is defined as the space between the impeller edge and the inboard chamber. The meters with tip clearance of 2 mm, 2.5 mm and 3 mm are considered. Table 2 shows the results of experiment and calculation with different tip clearances. The inner flow fields of the numerical simulation are shown in Figs.5-7.

Table 2 Comparison of different tip clearances

Clearance (mm)	2	2.5	3
Parameter	n (rpm)	n	n
Experiment	623	608	598
Calculation	600	574	560

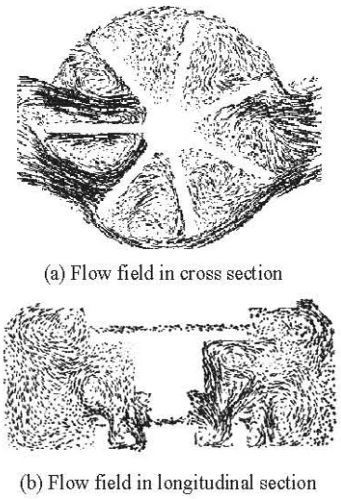

Fig.5 Flow fields with 2 mm of tip clearance

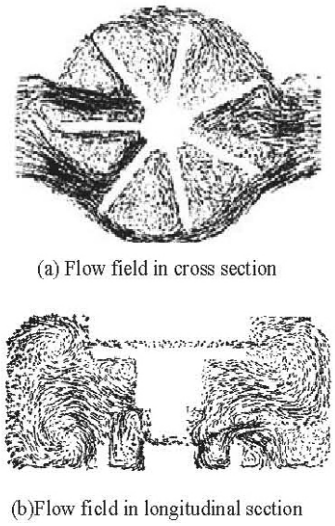

Fig.6 Flow fields with 2.5 mm of tip clearance

As shown in Table 2, with the same flux (2.5 m^3/h), the rotational speed of the impeller (n) is reduced with the increase of tip clearance. There are two reasons for this change: First, the decrease of the impeller diameter leads to a reduced area to be impacted by water flow, so the moment on the impeller is reduced. Second, with the increase of tip clearance, the leakage flow from the tip clearance also increases, with more fluid passing through the meter without impacting the impeller.

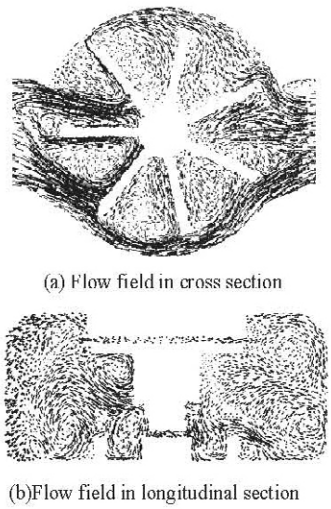

Fig.7 Flow fields with 3 mm of tip clearance

From Figs.5-7, the leakage flux by the tip clearance increases with the increase of tip clearance, with more water flow passing through the heat meter without impacting the impeller. Because of the influence of leakage flow on the impeller, the strong leakage vortex is produced and the angular speed of the impeller is reduced.

The influence of tip clearance on pressure loss is shown on Fig.8. Pressure loss reduces with the increase of tip clearance. With tip clearance increasing, the impeller area impacted by water flow decreases and the energy loss decreases, which causes a reduced pressure loss.

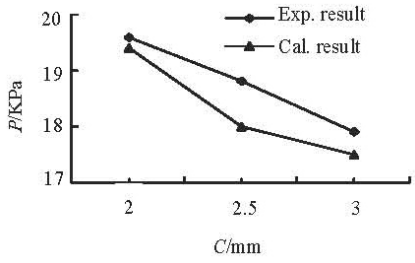

Fig.8 Pressure loss vs. clearance

6.3 *Influence of bottom ribs*

In order to study the influence of bottom ribs (as shown in Fig.9) on the heat meter, a meter without bottom ribs is also calculated in this article.

The flow field without bottom ribs is shown in Fig.10. In this case, water flows around the axis (as shown in Fig.9). Compared with the flow field with bottom ribs (Fig.11), the drag force of bottom flow is reduced, which may increase the effect of water

impacting impeller. The result of calculation also confirms this influence — the rotational speed of the impeller without bottom ribs is 750 rpm.

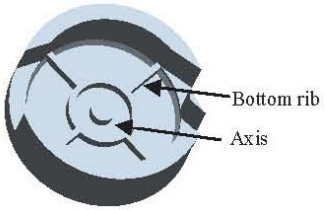

Fig.9 Bottom ribs

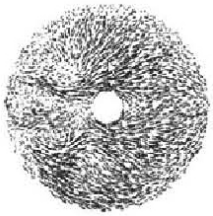

Fig.10 Flow field without ribs

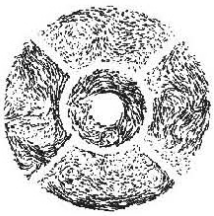

Fig.11 Flow field with ribs

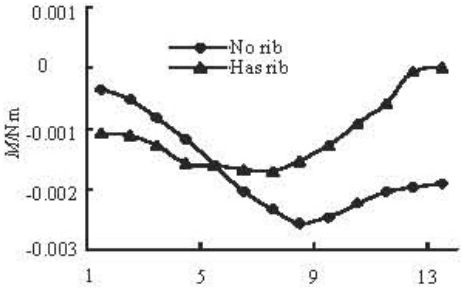

Fig.12 Axis moments of two different cases

The axis moments of two different cases are analyzed. Figure 12 shows the impeller rotary moment during turning one cycle. The results show that the rotary movement with bottom ribs is more stable than that without ribs at the direction of axis. Because of bottom ribs, the uniform swirls may form at the bottom, and these swirls act as the air-chamber to support the impeller on the axial direction, which makes the impeller revolution more stable.

6.4 *Influence of inlet swirl*

Because of different practical working conditions, different swirls may form at the inlet of the meter, which would influence the flow field. In order to simulate the practical situation, a swirl is added to the inlet flow in calculation.

Fig.13 Swirl section of outlet

The outlet cross section (Fig.13) is used in the calculation of the inlet velocity. This section abutted on the outlet of the chamber is the section with the strongest swirl. Then the calculation is reinitialized with the swirl added to the inlet velocity.

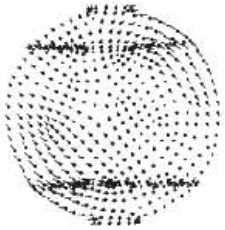

Fig.14 Section abutted on the inlet of the chamber

Calculated results show that the swirl of inlet influences the rotational speed of the impeller. The speed without inlet swirl is 600 rpm, but is 550 rpm when a swirl is added to the inlet, with 8.3% of relative error, so measures should be taken to reduce this influence.

In section 2 of this article, the length of inlet straight tube of the model is four times as the diameter of the pipe. Figure 14 shows the section abutted on the inlet of the chamber. Comparing Fig.13 with Fig.14, it is obvious that the swirl is reduced by passing through the inlet straight tube, and it is indicated that the straight tube with a length 4 times of the diameter can effectively reduce the influence of inlet swirl on the heat meter.

7. Conclusions

(1) In this article, a new method to calculate the impeller rotational speed is developed by the UDF technology, and its validity is shown by comparing the

obtained results with the results of Ref.[11].

(2) Research shows that the RNG $k-\varepsilon$ model is more effective for the calculation of inner flow with rotary wing mechanism.

(3) The increase of tip clearance can decrease the rotational speed of the impeller and reduce the loss of pressure between the inlet and outlet.

(4) Bottom ribs can reduce the rotational speed of the impeller, and it also can make the impeller rotate more stably.

(5) It is shown that the inlet swirl affects the stability of the heat meter. One method to solve this problem is to make the length of the inlet straight tube 4 times as the diameter.

References

[1] GUO Ge, DU Hong-lin and YAN Ji-hong et al. Technical status quo of thermal metering instrumentations and its prospect[J]. **Journal of Gansu University of Technology,** 2003, 29(2): 81-85(in Chinese).

[2] MÓCZÁR G., CSUBÁK T. and VÁRADY P. Distributed measurement system for heat metering and control[J]. **IEEE Transactions on Insturmentation and Measurement,** 2002**,** 51(4): 691-694.

[3] SHOJI K., TETSUO N. An electronic integrating heat meter[J]. **IEEE Transactions on Instrumentation and Measurement,** 1990, 39(5): 785-789.

[4] BABUS'HAQ R. F., OVERGAARD G. and PROBERT S. D. Heat-meter developments for CHP-DH networks[J]. **Applied Energy,** 1996, 53(1-2): 193-207.

[5] GUO Peng-cheng, LUO Xing-qi and ZHENG Xiao-bo et al. Numerical investigation of three-dimension turbulent flow fields in a Francis turbine[J]. **Journal of Hydrodynamics, Ser. A,** 2006,21(2): 181-189(in Chinese).

[6] CHEN Hong-xun. Research on turbulent flow within the vortex pump[J]. **Journal of Hydrodynamics. Ser. B,** 2004,16(6): 701-707.

[7] LI Yao-jun, WANG Fu-jun Numerical investigation of performance of an axial-flow pump with inducer[J]. **Journal of Hydrodynamics. Ser. B,** 2007, 19(6): 705-711.

[8] DU Guang-sheng, LIU Zheng-gang and LI Li et al. Fluid characteristics of rotary wing heat meter with single-channel[J]. **Journal of Hydrodynamics,** 2008, 20(1): 101-107.

[9] DU Guang-sheng, LIU Li-ning and LI Li et al. The influence of installation conditions of heat meters on interior fluid field and flux measurement accuracy[C]. **Proceedings of The Conference of Global Chinese Scholars on hydrodynamics.** Shanghai, 2006, 455-460.

[10] DU Guang-sheng, WANG Ning and LIU Zheng-gang et al. Fluid characteristic study on rotary wing heat meter with two-stream[J] **Chinese Journal of Scientific Instrument,** 2006, 27(9): 1071-1074(in Chinese).

[11] LIU Zheng-gang, Du Guang-sheng and WANG Ning et al. Research on fluid characteristic within the rotating-wing heat meter[J]. **Journal of Hydrodynamics, Ser. B,** 2006, 18(4): 458-463.

[12] WANG Ning. A fluid characteristic study on rotary wing heat meter with two-stream[D]. Master Thesis, Jinnan: Shandong University, 2005(in Chinese).

[13] TAO Wen-quan. **Numerical heat transfer**[M]. Xi'an: Xi'an Jiaotong University Press, 1988(in Chinese).

[14] DU Guang-sheng. **Engineering hydrodynamics**[M]. Beijing: China Electric Power Press, 2005(in Chinese).

[15] WANG Fu-jun. **Analyse of computational fluid dynamics**[M]. Beijing: Tsinghua University Press, 2004(in Chinese).

[16] FERZIGER J. H., PERIC M. **Computational methods for fluid dynamics**[M]. Berlin,German: Springer, 2002.

[17] WANG Yuan-cheng, WU Weng-quan. Numerical simulation of flow around square cylinder using RNG $k-\varepsilon$ turbulence model[J]. **Journal of Hydrodynamics. Ser. A,** 2004, 19(Suppl.): 916-920(in Chinese).